the cases studied. Both the ABSFOM and RESID figures of merit were found to be good indicators of the best phase sets. PSIZERO was also found to be acceptably good despite the fact that reflexions with zero $\Delta_{ano}$ cannot be reliably identified. The missing centric data did not prevent success in these trials. Further work is needed to see if the technique will handle many anomalous scatterer sites as might occur with genetically engineered proteins.

We are grateful to a number of people for supplying data sets. Dr M. Helliwell measured the small-molecule data and Mrs E. J. Dodson calculated the anomalous differences. Dr Z. Derewenda provided the mercury derivative $\alpha$-amylase data. Other data sets have already been referenced. Professors M. M. Woolfson and Fan Hai-fu are thanked for valuable discussions. We are grateful to the Science and Engineering Research Council for grant support.

### References

ADAMS, M. J., HELLIWELL, J. R. & BUGG, C. E. (1977). *J. Mol. Biol.* **112**, 183-197.

BLUNDELL, T. L. & JOHNSON, L. N. (1976). *Protein Crystallography*. New York: Academic Press.

DEBAERDEMAEKER, T., GERMAIN, G., MAIN, P., TATE, C. & WOOLFSON, M. M. (1987). *MULTAN87. A System of Computer Programs for the Automatic Solution of Crystal Structures from X-ray Diffraction Data*. Univ. of York, England.

EINSPAHR, H., SUGUNA, K., SUDDATH, F. L., ELLIS, G., HELLIWELL, J. R. & PAPIZ, M. Z. (1985). *Acta Cryst.* B**41**, 336-341.

GOMEZ DE ANDEREZ, D., HELLIWELL, M., HABASH, J., DODSON, E. J., HELLIWELL, J. R., BAILEY, P. D. & GAMMON, R. E. (1989). *Acta Cryst.* B**45**, 482-488.

HELLIWELL, J. R. (1984). *Rep. Prog. Phys.* **47**, 1403-1497.

HENDRICKSON, W. & TEETER, M. (1981). *Nature (London)*, **290**, 107-113.

WILSON, K. S. (1978). *Acta Cryst.* B**34**, 1599-1608.

*Acta Cryst.* (1989). A**45**, 718-726

# Combined Use of Monochromatic and Laue Diffraction Techniques for Macromolecular Structure Determination

BY H. D. BARTUNIK AND T. BORCHERT

*Max-Planck Society, Research Unit for Structural Molecular Biology, c/o DESY, Notkestrasse* 85, 2000 *Hamburg* 52, *Federal Republic of Germany*

(*Received* 25 *October* 1988; *accepted* 1 *June* 1989)

### Abstract

A novel strategy of macromolecular structure analysis is described which combines the use of monochromatic scanning Laue (SCL) and white-beam Laue (WBL) diffraction techniques. It provides, when applied with an area detector with on-line capabilities, a means of interactively determining and optimizing experimental parameters; it further makes rapid data evaluation feasible, also with off-line detector systems. These new procedures have been applied to a protein structure, $\beta$-trypsin, using a FAST area detector (Enraf-Nonius) and image plates (Fuji) on a double-focusing synchrotron beamline at DORIS. Structure factors, which were derived from FAST Laue data, were empirically scaled by comparing equivalent reflections in different wavelength bins. A $2F_o - F_c$ difference Fourier map, which was calculated at 1·8 Å resolution using these structure-factor moduli together with phases from the known structural model, showed well defined electron density distribution ($R = 22\%$). Image-plate exposures showed diffraction to 1·2 Å resolution. The effect of crystal mosaicity on the maximum wavelength bandwidth for Laue exposures has been investigated. SCL techniques, which involve rapid scanning (with a crystal or multilayer monochromator or a tunable undulator) through a defined wavelength range, extend the applicability of Laue techniques to crystals with broadened mosaic spread.

## 1. Introduction

Laue diffraction techniques provide a means of measuring integrated reflection intensities for crystal structure analysis by exposure of a stationary crystal to an incident (neutron or X-ray) beam of broad spectral distribution (Lowde, 1956; Buras, Mikke, Lebech & Leciejewicz, 1965). They were first employed in the neutron structure determination of small biological structures (Hohlwein, 1977; Klar, Hingerty & Saenger, 1980) using a modified Laue technique (Maier-Leibnitz, 1967). The same technique was used in the first (neutron) Laue diffraction study of a protein structure (Hohlwein & Mason, 1981). It was recently demonstrated that Laue techniques could be applied in protein diffraction studies with syn-

0108-7673/89/100718-09$03.00 

chrotron radiation (SR) thus exploiting its 'white-beam' characteristics (Moffat, Szebenyi & Bilderback, 1984; Cruickshank, Helliwell & Moffat, 1987; Hajdu *et al.*, 1987; Farber, Machin, Almo, Petsko & Hajdu, 1988). The high brilliancy of SR sources makes very short exposure times feasible. In the case of cyclicly repeatable protein reactions, monochromatic techniques may be employed on a μs to ms time scale; in theory, even ns resolution may be reached when exploiting the pulsed time structure of SR (Bartunik, 1983). Laue diffraction techniques extend the range of applications to non-cyclic reactions, in particular to many enzymatic reactions (Hajdu, Acharya, Stuart, Barford & Johnson, 1988). This has led to an increasing interest in the further development of Laue techniques and instrumentation (*e.g.* Helliwell *et al.*, 1989).

Although programmes have been developed for processing of Laue exposures (on photographic film) without previous knowledge of the exact crystal orientation (Machin, 1987), such (off-line) data evaluation may involve a rather long time. In view of the fact that applications of Laue methods to the study of conformational changes in proteins would often require quite complicated auxiliary techniques (*e.g.* for initiating reactions by laser photoactivation of inactive metabolites to active metabolites), interactive control of the experiment and on-line evaluation of Laue exposures is of considerable interest. We have followed a novel approach to Laue data collection and evaluation which provides such interactivity and immediate processing possibilities. Prior to broad-bandpass Laue exposures, the crystal orientation, mosaicity and diffraction limit are determined and experimental parameters are optimized by monochromatic and SCL techniques using an area detector system with on-line capabilities and high quantum detection efficiency. Thus a means is provided for reliable prediction of subsequently recorded Laue patterns, even if these (SCL or WBL) exposures are taken using another, off-line, detector medium [like the imaging plate (Amemiya *et al.*, 1988)].

This new strategy has been tested out in an application to a protein structure, β-trypsin, which was previously determined by conventional techniques (Marquart, Walter, Deisenhofer, Bode & Huber, 1983). With a double-focusing synchrotron beamline, X31 at EMBL/DORIS, it was possible to switch between monochromatic and polychromatic diffraction conditions without dismounting the sample crystal. Interactivity was provided through the use of a FAST detector system. Laue data were also recorded on Fuji image plates. The aim of the presently described experiment was to investigate prediction, processing and scaling methods; no emphasis was laid on short exposure times (in contrast to Laue experiments which were subsequently carried out on a wiggler station at DORIS and will be described elsewhere).

Laue prediction and evaluation routines have been developed. The prediction takes the effects of crystal mosaicity on the wavelength excitation range of reflections and on the reflection spot size on the detector screen into account. The applicability of Laue methods to crystals with broadened mosaic spread has been investigated. The concepts and techniques are described together with the results of the test application.

## 2. Prediction and processing of Laue diffraction patterns

A program package (*LAUEMAD*) has been developed for Laue data prediction, collection and processing. It was initially written for use with a FAST area detector system and has been extended to the application of X-ray-sensitive photographic film and of image plates. *LAUEMAD* is partly based on the (monochromatic) data collection program *MADNES* (Messerschmidt & Pflugrath, 1987). The basic concepts of the routines in *LAUEMAD* which relate to polychromatic diffraction and of wavelength-dependent scaling of structure factors are described in the following.

### 2.1. *Prediction of reflection position and wavelength range*

For a mathematical description of Laue diffraction geometry (Fig. 1), an orthogonal coordinate system in reciprocal space has been used with the $z$ axis antiparallel to the direction of the incident beam and the $x$ axis pointing downwards. Circles with radii $R_{max}$, $R_{min}$ represent the Ewald spheres for the limiting wavelengths $\lambda_{min}$ and $\lambda_{max}$, respectively. Reciprocal-lattice points which are located between both spheres fulfil the conditions for diffraction.

Reasonable estimates of $\lambda_{min}$ and $\lambda_{max}$, the crystal diffraction limit, $d_{min}$, and the crystal mosaicity are required for reliable prediction and processing of

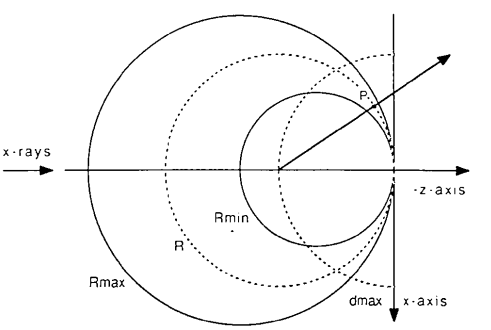


Fig. 1. Laue diffraction geometry. The diffracting volume of reciprocal space is limited by the Ewald spheres with radii $R_{max}$ and $R_{min}$, and by the resolution sphere with radius $d_{min}$.

Laue patterns. In the SCL method, $\lambda_{min}$ and $\lambda_{max}$ are precisely defined; hence, empirical determination of the other parameters is greatly facilitated. In general, the effective wavelength limits in WBL studies are only approximately known; they are (as soft limits) defined by the spectral distribution of the synchrotron, by (short-wavelength) cut-offs through X-ray optical elements like mirrors and (on the long-wavelength side) by absorption effects.

Crystal mosaicity and divergences in the incident beam cause broadening in the range of wavelengths which contribute to the total intensity in a given reflection in a Laue pattern. In a first approximation (Greenhough & Helliwell, 1982), the beam divergence and mosaic spread combine to give an effective mosaic spread, $\mu$, and the resolution function for a given reciprocal-lattice point at distance $d^*$ from the origin is assumed to be a sphere of radius $S$,

$$S = 0{\cdot}5\ \mu\ d^* \cos\theta,$$

where $\theta$ is the Bragg angle of the corresponding reflection. The range of wavelengths, $\lambda_1 < \lambda < \lambda_2$, contributing to the excitation of the reflection is given by

$$\lambda_2 - \lambda_1 = 4S/(d^{*2} - S^2).$$

In broad-bandpass applications, relatively few reflections are partials, *i.e.* their resolution spheres are not fully contained between the limiting Ewald spheres (with radii $R_{min}$, $R_{max}$), and may be neglected compared with the number of fully excited reflections.

Theoretical distribution of reflections in Laue diffraction which are affected by energy overlaps, *i.e.* by superposition of multiple orders, was investigated by Cruickshank *et al.* (1987).

### 2.2. *Prediction of the reflection spot size*

The prediction routines take the spatial extent of reflection spots on the detector into account in order to handle spatial overlaps adequately. An estimate of the spot size is derived from a projection of the spherical resolution function onto a plane. For a reflection excited by wavelengths within the range $\lambda_1 < \lambda < \lambda_2$ around a central wavelength $\lambda_c$, the angular width of the reflected beam may be described by the components $\tau_1$ in the scattering plane and $\tau_2$ in the direction perpendicular to the scattering plane.

$$\tau_1 = \cos^{-1}[1 - (S^2\lambda_c^2)/2]$$

$$\tau_2 = \cos^{-1}[1 - K\lambda_2^2/(1 + S\lambda_2)] - \cos^{-1}[1 - K\lambda_1^2/(1 - S\lambda_1)]$$

where $K = (d^{*2} - S^2)/2$.

The radius of the resolution sphere is, as above, assumed to vary linearly with the mosaic spread. Fig. 2 shows examples of patterns predicted for a protein structure (trypsin; wavelength range 0·7–1·5 Å; diffraction limit $d_{min} = 1{\cdot}5$ Å). Figs. 2(*a*) (mosaic spread 0·15°) and (*b*) (0·4°) relate to the use of a detector (like the FAST) with 512 × 512 pixels at a distance of 69 mm. The variation in the numbers of useful, overlapping and partial reflections as functions of increasing mosaic spread is displayed in Fig. 3. Figs. 2(*c*)–(*e*) (mosaic spread angles 0·1, 0·3 and 0·5°, respectively) correspond to a distance of 210 mm and refer to detectors (like image plates) with 1500 × 1500 pixels. For both detector types, further broadening of the reflection spots due to a cross section of the incident beam of 100 μm and a detector point-spread function of 100 μm has been taken into account. The effect of crystal mosaicity on the reflection spot size in Laue diffraction from small structures was previously estimated by Harding and co-workers (Andrews, Hails & Harding, 1987).

### 2.3. *Optimization of wavelength bandwidth*

The maximum allowed wavelength bandwidth depends strongly on the crystal mosaicity. This dependence has been investigated for the example of a trypsin crystal in a given orientation relative to the

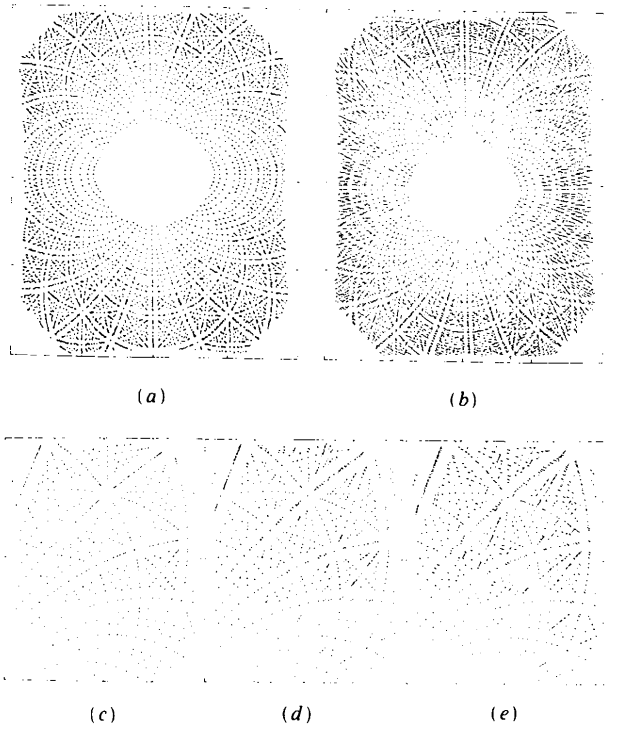


Fig. 2. Prediction of reflection spots for a Laue exposure from the BPT structure (*b* axis parallel to the incident beam; the crystal parameters are described under § 3.1). Spot sizes are indicated by the main axes of their projected resolution ellipsoids. Parameters: wavelength range 0·7–1·5 Å; diffraction limit $d_{min} = 1{\cdot}5$ Å; beam cross section 100 μm. (*a*) and (*b*) correspond to a detector with 512 × 512 pixels and a crystal-to-detector distance of 69 mm. (*c*)–(*e*) show a section of the pattern predicted for 1500 × 1500 pixels and 210 mm. Mosaic spread angle: (*a*) 0·15, (*b*) 0·4, (*c*) 0·1, (*d*) 0·3 and (*e*) 0·5°.

incident beam. In Fig. 4, the number of useful reflections is displayed against the bandwidth assuming a maximum wavelength of 1·5 Å.

### 2.4. *Derivation of structure factors*

The relationship between the structure-factor modulus, $|F(hkl)|$, and the integrated reflection intensity, $I(hkl)$, is given by (Zachariasen, 1945)

$$I(hkl) = I_o Q \mathrm{d}V$$

$$Q = (e^2/mc^2V)^2 PL|F(hkl)|^2$$

where $I_o$ is the incident intensity, $\mathrm{d}V$ the crystal volume, $V$ the volume of the unit cell and $L$ the Lorentz factor,

$$L = \lambda^4/\sin^2\theta.$$

The polarization factor $P$ has been derived by Kahn *et al.* (1982) for the case of (linearly polarized) SR.

### 2.5. *Wavelength scaling*

The measured reflection intensities contain a number of wavelength-dependent factors. Apart from the Lorentz factor, these are primarily the spectral variation in the incident beam, absorption effects and the detector response. Extinction effects have not yet been observed and probably may be neglected in protein diffraction studies. In the present study, structure factors were scaled - after application of Lorentz and polarization corrections - in an empirical way. The data set was subdivided into 0·1 Å wide wavelength bins; an averaged scaling factor was derived for each bin relative to other bins by comparison of equivalent reflection intensities using the scaling routines of the program package *PROTEIN* (Steigemann, private communication). Linear interpolation between these bin scale factors produced the final wavelength-dependent scaling factors which were applied in order to set all structure factors onto a common scale.

In theory, dispersion effects in the atomic unscattering factors have also to be taken into account. When an upper wavelength limit near 2 Å is considered, anomalous contributions from sulfur and heavier atoms may be significant. Laue exposures may thus provide information both on the moduli and phases of structure factors.

## 3. Experiments and results

The new procedures of Laue data collection and evaluation have been tested out in an application to a protein structure, bovine pancreatic trypsin (BPT). Laue data were collected using both the scanning and the white-beam technique. The data were recorded with a TV-camera-type area detector system (FAST/Enraf-Nonius). In addition, Laue data were also recorded on image plates. The results which are described below have been derived from SCL and WBL applications with the FAST.

### 3.1. *Trypsin crystals*

Bovine pancreatic $\beta$-trypsin (BPT) was crystallized in the orthorhombic space group $P2_12_12_1$ ($a = 54·8$, $b = 58·4$, $c = 67·6$ Å) as previously described (Bode & Schwager, 1975). The outer dimensions of crystals used in the Laue diffraction experiments were about $0·3 \times 0·4 \times 0·8$ mm.

### 3.2. *Synchrotron data collection*

Both monochromatic and polychromatic diffraction data were collected from BPT crystals on the beamline X31 of the EMBL Outstation at DORIS/HASYLAB. The X-ray optics of this instrument include an Si(111) channel-cut monochromator and a 1:1 double-focusing Au-coated mirror. Despite the mirror, the vertical and horizontal divergences in the incident beam are small, owing to a 17 m long

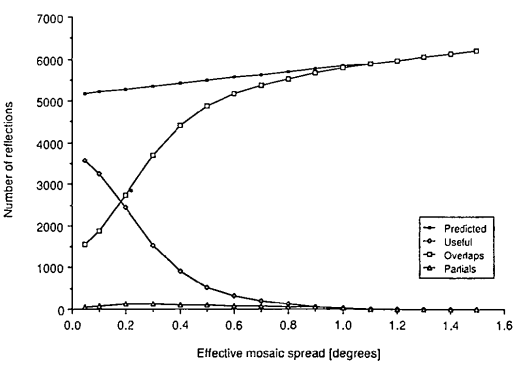


Fig. 3. Effect of broadened crystal mosaicity on the number of useful (*i.e.* non-overlapping fully excited) reflections which may be observed in a Laue experiment. Parameters are the same as for Fig. 2, except for a take-off angle of 11·8° of the detector relative to the incident beam.

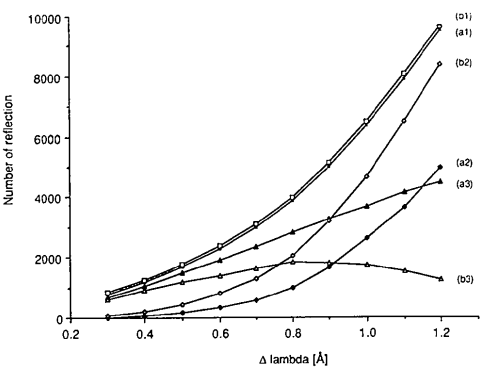


Fig. 4. Effect of increasing wavelength bandwidth, $\Delta\lambda$, on the number of useful reflections. A maximum wavelength of 1·5 Å and an effective mosaic spread angle of (*a*) 0·1 and (*b*) 0·3°, respectively, are assumed. Otherwise, parameters as for Fig. 3. Index 1 denotes general, 2 overlapping and 3 useful reflections.

distance between mirror and sample positions. A 0·1% wavelength bandpass was used in the monochromatic and SCL exposures. DORIS was running under 'parasitic' conditions (5 GeV; single-bunch mode; maximum electron currents of 50 mA; lifetimes of about 1 h).

*Orientation matrix determination by monochromatic techniques.* The orientation matrix of the sample crystal was determined and - together with the relevant experimental and instrumental parameters - refined on the basis of a series of short crystal rotation exposures (of a few seconds each) with the FAST using monochromatic radiation at a wavelength of 1·009 Å.

*SCL diffraction.* For the SCL exposures, the monochromator was scanned through a wavelength range of $1{\cdot}009 < \lambda < 1{\cdot}488$ Å. Since the X31 monochromator does not provide a constant-height exit, the X-ray optics were optimized at an intermediate wavelength near 1·2 Å with respect to the intensity incident on the sample. SCL data were measured from a series of (stationary) crystal orientations corresponding to 5° steps in a rotation through a 90° range around an axis perpendicular to the direction of the incident beam. Each scan took 50 s.

*White-beam Laue diffraction.* The channel-cut monochromator at X31 has a gap width of 5 mm. Through this gap, a small part (around 5%) of the incident white beam was extracted and reflected by the double-focusing mirror which has a short-wavelength cut-off at about 0·6 Å. On the long-wavelength side, absorption effects (due to Be windows, air paths and sample) cause strong suppression of wavelengths above 2 Å. Exposure times varied between 1 and 30 s for data collection to very high resolution; nearly identical exposure times were used with the FAST detector and with Fuji imaging plates. Fig. 5 shows a WBL exposure taken with the FAST from a trypsin crystal oriented with a principal axis approximately parallel to the incident beam. The crystal-to-detector distance was 70 mm and the exposure time was 30 s. Data extend to a resolution of 1·5 Å. A subsequent exposure under the same conditions, except for a distance of 140 mm, was recorded on a Fuji image plate. Fig. 6 shows the image after laser scanning and digitization; here, the data extend even to 1·2 Å resolution.

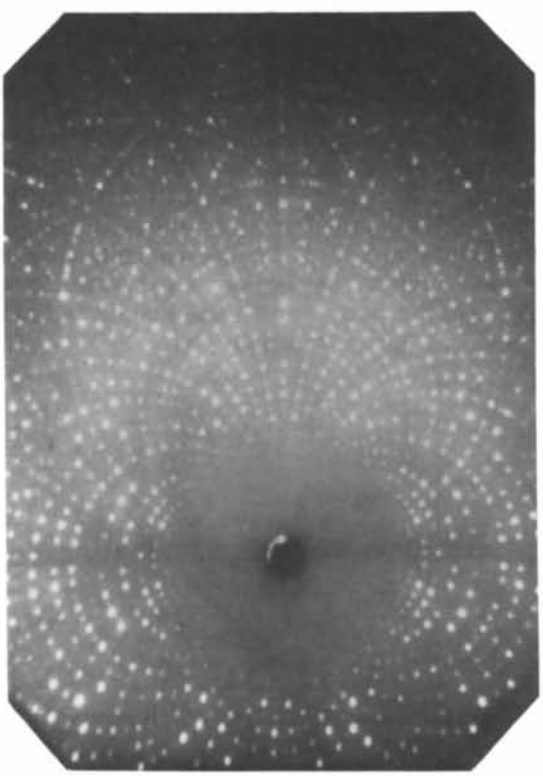

Fig. 5. White-beam Laue exposure recorded on the FAST detector from a BPT crystal mounted with its *b* axis approximately parallel to the incident beam. Crystal-to-detector distance 69 mm, detector take-off angle 11·8°, exposure time 30 s. Short-wavelength cut-off near 0·6 Å.

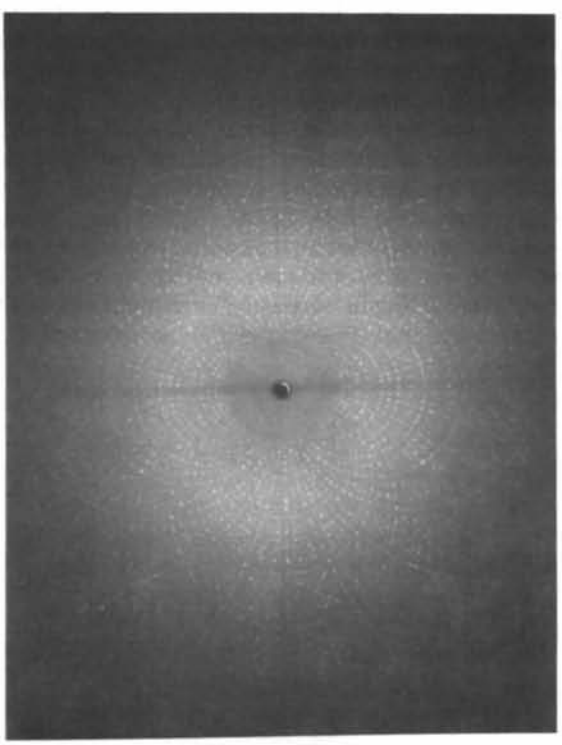

Fig. 6. White-beam Laue exposure on an image plate taken under identical conditions as for Fig. 5, except for a crystal-to-plate distance of 100 mm. The image plate (size 200 × 250 mm) has been scanned with a 100 μm raster and digitized on a logarithmic 8-bit scale (which enhances the apparent background level).

The diffraction quality of the BPT crystals did not show any degradation during the WBL exposures. In later experiments which were carried out on X31 with significantly higher incident SR intensity, exposure times for WBL diffraction from BPT to similar resolution were reduced to a few tenths of a second, and effects of radiation damage were strongly enhanced. These experiments will be described elsewhere.

*Area detectors.* The FAST (TV-type) detector system (Enraf–Nonius) was mounted on a two-circle goniometer. The spindle axis and the beam monitoring were controlled by an LSI11 *via* CAMAC. The FAST was controlled by a MicroVAX II. Synchronization of both processors was achieved *via* a data link. The program *MADSYN* (Borchert, Prei-Rueffer, Schmalzl & Bartunik, private communication), which is a modified version of *MADNES* (Messerschmidt & Pflugrath, 1987) was used for monochromatic data collection and crystal orientation refinement. The program *LAUEMAD* described above was used in the SCL and WBL data collection.

SCL and WBL Laue data were also recorded on Fuji image plates with an active area of 200 × 250 mm. The plates were scanned with a 100 × 100 μm raster on a laser scanner (Philips Medizin-Systeme, Hamburg). The data were digitized into 8 bits on a logarithmic scale.

### 3.3. *Results of scanning Laue diffraction experiments*

The Laue patterns were predicted on the basis of the orientation matrix determined previously (by monochromatic techniques). The crystal mosaic spread angle, $\mu$, refined to values around 0·15°. This prediction turned out to be very accurate; the Laue data could thus be processed without further refinement of crystal orientation and experimental parameters.

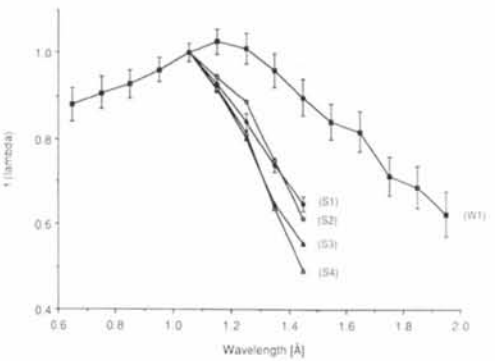


Fig. 7. (Inverse) wavelength normalization curve as obtained from internal scaling of symmetry-equivalent reflections. (S1) to (S4) correspond to SCL exposures (scan range of 1·0–1·5 Å) which were subsequently taken within a total time of 30 min during one fill of DORIS. Curve W1 has been derived from the WBL image displayed in Fig. 5.

The data were reduced and scaled in wavelength bins following the procedure described above. In Fig. 7, the scaling factors as obtained from the wavelength scaling procedure are displayed *versus* the wavelength bins for SCL exposures and, for comparison, from a WBL exposure. The wavelength dependence of the scaling factors varies from one SCL exposure to the other. One observes in particular a systematic change from the first exposure to the second *etc.* taken during one fill of the synchrotron. This indicates a dependence on the primary intensity in the white beam incident on the scanning monochromator. It may be qualitatively explained by heating effects inducing intensity and take-off-angle-dependent mistuning of the channel-cut monochromator crystal. Fig. 8 gives statistics of the processed SCL data. In total, 35% of all possible reflections to 1·8 Å resolution were obtained. The merge $R$ factor measuring the agreement between all symmetry-related reflections was 12% based on intensities. In general, better agreement was obtained for symmetry-related reflections which were observed (within different wavelength bins) on one and the same exposure; these $R_{sym}$ values varied between 5 and 10%.

The structure-factor moduli derived from the scanning Laue measurements were compared to the structural model (*DEBA*) of BPT (Marquart *et al.*, 1983). The crystallographic $R$ factor is 0·22 at 1·8 Å resolution. Fig. 9 shows a section of a $2F_o - F_c$ electron density map which was calculated with *DEBA* phases at 1·8 Å resolution.

### 3.4. *Results of white-beam Laue diffraction experiments*

WBL exposures taken with the FAST were processed in a very similar way to the SCL data. The

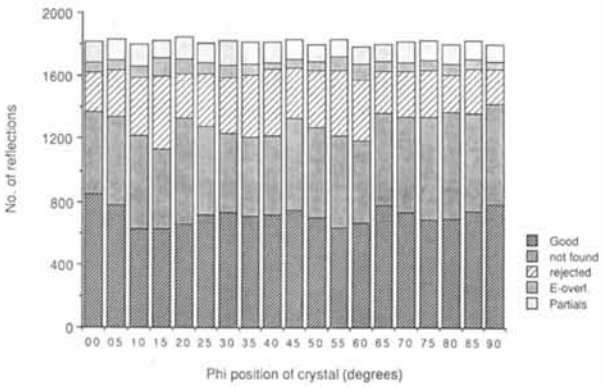


Fig. 8. Statistics of the processing of Laue data taken in a series of SCL exposures (scan range 1·0–1·5 Å) from a stationary BPT crystal at 5° intervals of a rotation through 90° around the *a* axis. Data have been recorded on the FAST with parameters as for Fig. 3. Exposure time 50 s. Classification of reflections was based on pattern prediction to 1·5 Å resolution. Overlaps refer in the figure to energy overlaps, whereas spatial overlaps are contained in the number of rejected reflections.

limiting wavelengths, $\lambda_{min}$ and $\lambda_{max}$, were empirically determined through comparison of predicted and observed patterns. The resulting value for $\lambda_{min}$ agrees rather well with the short-wavelength cut-off (near 0·6 Å) of the X-ray mirror. The number of observed reflections decreases rapidly for wavelengths above 2·0Å.

Evaluation of a FAST white-beam picture yielded quite a good $R$ factor of 7% with about 2500 reflections (1200 unique) in one image. The wavelength scaling curve which resulted from the scaling procedure described above is shown in Fig. 7.

## 4. Discussion

The combined use of monochromatic and polychromatic diffraction techniques has been functional in both the data collection and evaluation parts of the Laue experiment. The fact that the crystal orientation matrix was determined (with monochromatic radiation) prior to polychromatic exposures made reliable prediction of Laue diffraction patterns quite straightforward. This and on-line capabilities of the FAST detector system made it possible to compare predicted and observed patterns immediately. Thus, interactivity was provided in the optimization of experimental conditions like exposure times, crystal-to-detector distance and the wavelength range, and further in the estimation of parameters which are crucial for data processing, in particular the crystal diffraction limit, its mosaic spread and (in the case of WBL exposures) the effective wavelength range. These advantages remain significant, even if Laue exposures are subsequently recorded on another, off-line, detector medium like - as in part of the present experiment - imaging plates in order to make use of a higher number of pixels and broader dynamical range. Determination of the crystal orientation could in theory be based on a single exposure to a monochromatic (or small-bandpass) beam. The radiation damage caused by such setting exposures may be neglected with detectors of high quantum detection efficiency. The suggested procedure therefore appears to be generally applicable on white-radiation beamlines which are equipped with a removable monochromator.

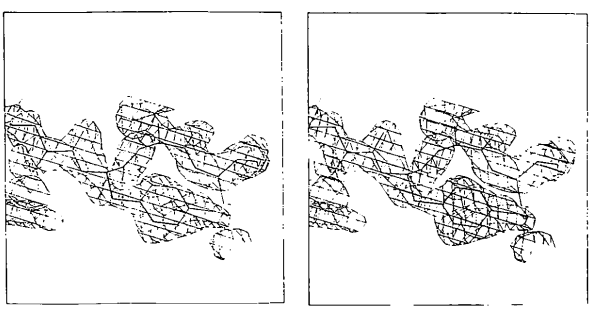

Fig. 9. $2F_o - F_c$ electron density map of BPT calculated with structure-factor moduli which were derived from SCL data and with phases corresponding to the known structural model (Marquart *et al.*, 1983). The plot shows a section of the map with superimposed model coordinates near residue Tyr 94.

The success in the (test) application of the new strategy and routines to protein structure analysis at high resolution manifests itself in a relatively good crystallographic $R$ value of 22% and in the quality of the $2F_o - F_c$ difference Fourier map (Fig. 9) of the BPT structure at 1·8 Å resolution, prior to structural refinement. Side chains and even water molecules are quite well defined, despite the lack of completeness in the data set. The structure factors which were used in the calculation of the electron density map resulted from SCL exposures taken with an exactly defined wavelength range. The presently described method is, however, also applicable with white radiation. In fact, the data derived from a WBL exposure were of significantly higher accuracy than from the corresponding SCL exposure. This difference is probably mainly due to a reduction in the intensity of the incident beam which results in underexposure of a greater number of reflections; it may be avoided with an improved (constant-exit-height and cooled) monochromator. The SCL exposures were taken at a number of different (stationary) crystal orientations in order to overcome the limitations in the number of pixels of the FAST. In theory, a sufficient number of structure factors for a Fourier synthesis at high resolution could be derived from a single exposure on an imaging plate.

The present study involved internal scaling of Laue data using a wavelength normalization curve which was empirically derived from comparison of symmetry-related reflections; such a procedure was also applied in a recent study by Hajdu and co-workers (Farber *et al.*, 1988). The WBL normalization curve in Fig. 7 shows relatively small (23%) variation across the wavelength range from 0·6 to 2·0 Å. This is partly explained by the slow variation with wavelength of the detection quantum efficiency of the FAST system (with a $Gd_2O_2S$ scintillator). When the calculated absorption efficiency of a BaFBr phosphor screen *versus* wavelength (Amemiya *et al.*, 1988) over the same range is considered, similar conditions are to be expected with image plates.

Extremely high Bragg resolution my be reached in broad-bandpass Laue data collection in the case of small-crystal mosaic spread. This is illustrated by Fig. 6 showing a WBL exposure (wavelength bandwidth 0·8 Å) from trypsin (mosaic spread 0·15°) on an image plate. Prediction of this pattern, based on parameters which were derived from an exposure on the FAST under identical conditions (except for another crystal-to-detector distance), indicates a diffraction limit corresponding to 1·2 Å resolution. This resolution is higher than the highest resolution

(1·4 Å) which has until now been observed in monochromatic diffraction from BPT crystals using SR.

The applicability of broad-bandpass Laue techniques is strongly reduced when the crystal mosaicity broadens as may, for example, transiently occur through coexistence of different structural states during enzyme–substrate interactions. An increase in the mosaic spread and hence in the reflection spot size results in a rapid decrease in the number of useful reflections and the formation of streaks (Figs. 2–3). For a structure with cell dimensions around 60 Å which diffracts to 1·5 Å resolution, the wavelength bandwidth has to be limited to less than 0·8 Å in order to obtain at least 25% useful reflections out of all possible if the mosaic spread reaches 0·3° (Fig. 4). This refers to a beam cross section of 100 μm and to area detectors with 512×512 pixels and a point spread function of 100 μm. If detectors (like image plates) with a much higher number (about 1500× 1500) of pixels are used at a correspondingly longer distance from the crystal, mosaic spread angles up to nearly 0·5° (when the resolution functions of neighbouring reciprocal-lattice points start to overlap) may be tolerated with such a bandwidth (Figs. 2*c–e*).

The wavelength range and bandwidth may be adjusted in case of broadened sample mosaic spreads by a number of techniques. A short-wavelength limit may be defined through the cut-off in the reflection from a mirror, as in the present study. A limited bandwidth of several percent may be obtained from undulators. Broader bandwidths which are required for efficient use of Laue techniques may possibly be produced by tunable undulators (Viccaro & Shenoy, 1988) or, on a wiggler, by scanning monochromator techniques. Rotating double-crystal monochromators with broadened mosaic spread or multilayer monochromator systems (Pianetta & Barbee, 1988) may be applied. The resolution function around reciprocal-lattice points extends over a wavelength range of the order of 1%; SCL exposure times are therefore longer by one to two orders of magnitude compared with exposure times with white-beam radiation. For the example of an incident intensity of the order of $10^{15}$ photons $s^{-1}$ in a 1% bandpass (as is estimated for a wiggler at DORIS assuming a double-focusing mirror and a current of 50 mA), an exposure time of 1 μs may be sufficient for WBL diffraction; this corresponds in single-bunch mode to an effective exposure time of the order of 100 ps. A multilayer monochromator with a *d* spacing of 30 Å rotating at 10 000 r $min^{-1}$ may scan a 0·6 Å wavelength band within 10 μs; such time scales may thus be accessible even in the case of broadened crystal mosaicity. Hence, conformational changes which occur during enzymatic reactions on μs to ms time scales may be studied with SCL techniques. White-beam Laue diffraction techniques may even make it feasible to reach the time resolution required, for example, for investigating the crystal structure of 200–300 ps intermediates in the photocycle of photosynthetic reaction centres.

We gratefully acknowledge the help of many scientists and colleagues. Dr Keith Wilson (EMBL, Hamburg) made the use of the beamline X31 and of a graphics system possible. Dr Youchiro Maeda (EMBL, Hamburg) let us use his image plates and instructed us about optimum exposure and scanning conditions. Dr U. Neitzel (Fa. Philips Medizin-Systeme, Hamburg) made a laser scanner available for digitization of image plate exposures. Sandra McLaughlin (EMBL, Hamburg) gave support to CAMAC programming. Birgit Hummel assisted in crystal preparation and mounting. We thank Dr Janos Hajdu (Univ. Oxford), Professor John Helliwell (Univ. Manchester), Professor Keith Moffat (Cornell Univ.), Dr John Campbell (SRS Daresbury) and Dr Wolfgang Jauch (HMI Berlin) for most valuable discussions. This work has been funded by the German Federal Minister for Research and Technology (BMF) under contract no. 05 180MP B O.

### References

AMEMIYA, Y., MATSUSHITA, T., NAKAGAWA, A., SATOW, Y., MIYAHARA, J. & CHIKAWA, J. (1988). *Nucl. Instrum. Methods*, **A266**, 645–653.

ANDREWS, S. J., HAILS, J. E. & HARDING, M. M. (1987). *Acta Cryst.* **A43**, 70–73.

BARTUNIK, H. D. (1983). *Nucl. Instrum. Methods*, **208**, 523–533.

BODE, W. & SCHWAGER, P. (1975). *J. Mol. Biol.* **98**, 693–717.

BURAS, B., MIKKE, K., LEBECH, B. & LECIEJEWICZ, J. (1965). *Phys. Status Solidi*, **11**, 567.

CRUICKSHANK, D. W. J., HELLIWELL, J. R. & MOFFAT, K. (1987). *Acta Cryst.* **A43**, 656–674.

FARBER, G. K., MACHIN, P., ALMO, S. C., PETSKO, G. A. & HAJDU, J. (1988). *Proc. Natl Acad. Sci.* **85**, 112–115.

GREENHOUGH, T. J. & HELLIWELL, J. (1982). *J. Appl. Cryst.* **15**, 338–351.

HAJDU, J., ACHARYA, K. R., STUART, D. I., BARFORD, D. & JOHNSON, L. N. (1988). *Trends Biol. Sci.* **13**, 104–109.

HAJDU, J., MACHIN, P. A., CAMPBELL, J. W., GREENHOUGH, T. J., CLIFTON, I. J., ZUREK, S., GOVER, S. & JOHNSON, L. N. (1987). *Nature (London)*, **329**, 178.

HELLIWELL, J. R., HARROP, S., HABASH, J., MAGORRION, B. J., ALLINSON, N. M., GOMEZ, D., HELLIWELL, M., DEREWENDA, Z. & CRUICKSHANK, D. W. J. (1989). *Rev. Sci. Instrum.* In the press.

HOHLWEIN, D. (1977). *Acta Cryst.* **A33**, 649–654.

HOHLWEIN, D. & MASON, S. A. (1981). *J. Appl. Cryst.* **14**, 24–27.

KAHN, R., FOURME, R., GADET, A., JANIN, J., DUMAS, C. & ANDRE, D. (1982). *J. Appl. Cryst.* **15**, 330–337.

KLAR, B., HINGERTY, B. & SAENGER, W. (1980). *Acta Cryst.* **B36**, 1154–1165.

LOWDE, R. D. (1956). *Acta Cryst.* **9**, 151–155.

MACHIN, P. A. (1987). Proc. Daresbury Study Weekend, DL/SCI/R25. SERC Daresbury Laboratory, Warrington, England.

MAIER-LEIBNITZ, H. (1967). *Ann. Acad. Sci. Fenn. Ser. A6*, p. 267.

MARQUART, M., WALTER, J., DEISENHOFER, J., BODE, W. & HUBER, R. (1983). *Acta Cryst.* **B39**, 480–490.

MESSERSCHMIDT, A. & PFLUGRATH, J. W. (1987). *J. Appl. Cryst.* **20**, 306–315.

MOFFAT, K., SZEBENYI, D. & BILDERBACK, D. (1984). *Science*, **233**, 1423–1425.
PIANETTA, P. & BARBEE, T. W. (1988). *Nucl. Instrum. Methods*, **A266**, 441–446.
VICCARO, P. J. & SHENOY, G. K. (1988). *Nucl. Instrum. Methods*, **A266**, 112–115.
ZACHARIASEN, W. H. (1945). *Theory of X-ray Diffraction in Crystals*. New York: Wiley.

*Acta Cryst.* (1989). **A45**, 726–732

# Genera of Minimal Balance Surfaces

BY WERNER FISCHER AND ELKE KOCH

*Institut für Mineralogie der Universität Marburg, Hans-Meerwein-Strasse, D-3550 Marburg, Federal Republic of Germany*

(*Received* 7 *April* 1989; *accepted* 1 *June* 1989)

## Abstract

The genus of a three-periodic intersection-free surface in $R^3$ refers to a primitive unit cell of its symmetry group. Two procedures for the calculation of the genus are described: (1) by means of labyrinth graphs; (2) *via* the Euler characteristic derived from a tiling on the surface. In both cases new formulae based on crystallographic concepts are given. For all known minimal balance surfaces the genera and the labyrinth graphs are tabulated.

## 1. Introduction

In a series of papers (Fischer & Koch 1987; 1989*a*, *b*; Koch & Fischer 1988, 1989*a*, *b*) minimal balance surfaces, *i.e.* three-periodic minimal surfaces subdividing $R^3$ into two congruent labyrinths, have been studied with respect to their symmetry properties. It turns out that the symmetry of a minimal balance surface is best described by a pair of space groups $G$–$H$, where $G$ represents the full symmetry of the surface and $H$ is that subgroup of $G$ with index 2 that does not interchange the two labyrinths and the two sides of the surface. Instead of space-group pairs proper black-white space groups may also be used (*cf.* Mackay & Klinowski, 1986; Fischer & Koch, 1987). New types of minimal balance surfaces have been derived making use of the fact that each twofold axis belonging to $G$ but not to $H$ has to lie within each minimal balance surface with symmetry $G$–$H$.

Within the cited papers for each minimal balance surface the fundamental topological constant called the genus has been given without an explanation of how it had been calculated. This will be given below.

## 2. The genus of a minimal balance surface

A non-periodic surface in $R^3$ is said to be of *genus* $g$, if it may topologically be deformed to a sphere with $g$ handles. According to this definition an ellipsoid and also a plane have genus 0, a torus (doughnut with one hole) genus 1, a pretzel (doughnut with two holes) genus 2 *etc.* Consequently, each three-periodic minimal surface has an infinite genus in this sense.

Therefore, a modified definition has been introduced for the genus of a three-periodic minimal surface (Schoen, 1970) counting only the number of handles per unit cell. In other words, the surface is embedded in a (flat) three-torus $T^3$ to get rid of all translations, and then the conventional definition of the genus is applied. The procedure of constructing $T^3$ from $R^3$ corresponds to identifying the opposite faces of the primitive unit cell [for a popular introduction to such manifolds see Weeks (1985)]. This may be visualized in analogy to transferring a two-periodic pattern in $R^2$ to the torus $T^2$ by rolling up a two-dimensional unit cell in both directions. In this approach an object moving within one labyrinth of the minimal surface and leaving the unit cell across one face will reenter it through the translationally equivalent opening on the opposite face. Obviously, the unit cell used has to refer to $H$, because otherwise the moving object thereby might change into the other labyrinth.

The genus of a three-periodic minimal surface may be calculated in different ways, two of which will be discussed here: (1) by means of the labyrinth graphs (Schoen, 1970; Hyde, 1989); (2) *via* the Euler characteristic determined with the aid of any tiling on the surface.

A third possibility makes use of the flat points of the surface (Hyde, 1989). As flat points are not easily discernible in all cases, however, it seems more appropriate to facilitate the search for flat points by the knowledge of the genus.

## 3. Labyrinth graphs

As a three-periodic minimal surface without self-intersection and the labyrinths separated by it are

0108-7673/89/100726-07$03.00 